



**HAL**  
open science

## **ROTKOKE: an assessment of macroscopic models for bcc Ni/Ni(100)**

Corina Etz, Andras Vernes, Peter Weinberger

► **To cite this version:**

Corina Etz, Andras Vernes, Peter Weinberger. ROTMOKE: an assessment of macroscopic models for bcc Ni/Ni(100). Philosophical Magazine, 2008, 88 (18-20), pp.2765-2775. 10.1080/14786430802395152 . hal-00513958

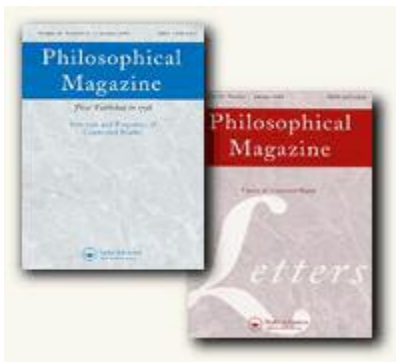
**HAL Id: hal-00513958**

**<https://hal.science/hal-00513958>**

Submitted on 1 Sep 2010

**HAL** is a multi-disciplinary open access archive for the deposit and dissemination of scientific research documents, whether they are published or not. The documents may come from teaching and research institutions in France or abroad, or from public or private research centers.

L'archive ouverte pluridisciplinaire **HAL**, est destinée au dépôt et à la diffusion de documents scientifiques de niveau recherche, publiés ou non, émanant des établissements d'enseignement et de recherche français ou étrangers, des laboratoires publics ou privés.



**ROTKOKE: an assessment of macroscopic models for bcc Ni/Ni(100)**

Journal:	<i>Philosophical Magazine &amp; Philosophical Magazine Letters</i>
Manuscript ID:	TPHM-08-May-0204
Journal Selection:	Philosophical Magazine
Date Submitted by the Author:	29-May-2008
Complete List of Authors:	Etz, Corina; Vienna University of Technology, Center for Computational Materials Science Vernes, Andras; Technical University Vienna, Center for Computational Materials Science Weinberger, Peter; Technical University Vienna, Centre for Computational Materials Science
Keywords:	magneto-optics, surface physics
Keywords (user supplied):	magneto-optical Kerr effect
<p>Note: The following files were submitted by the author for peer review, but cannot be converted to PDF. You must view these files (e.g. movies) online.</p> <p>PhilMag_ce08.tex</p>	



# ROTMOKE: an assessment of macroscopic models for bcc Ni/Ni(100)

C. Etz, A. Vernes, P. Weinberger

*Center for Computational Materials Science, Vienna University of Technology,  
Gumpendorferstr. 1a, A-1060 Vienna, Austria*

(Dated: May 29, 2008)

## Abstract

*Ab initio* Kerr angles for a multilayer system were calculated by means of Luttinger's formalism within the spin-polarized relativistic screened Korringa-Kohn-Rostoker method by including all multiple reflections and optical interferences via the  $2 \times 2$  matrix technique. Two further macroscopic models are suggested for a multilayer system, i.e., the two-media approach and the three-media approach. The Kerr angles obtained using the two-media approach show that 75 % of the Kerr rotation angles arise from surface contributions when compared to the  $2 \times 2$  matrix approach. Furthermore, by comparing the three-media approach to the  $2 \times 2$  matrix technique it is found that almost 25 % of the Kerr rotation angles are due to interfaces between the atomic layers.

PACS numbers: 75.70.Rf, 78.20.-e, 78.20.Ls, 78.66.Bz, 78.68.+m

Keywords: magneto-optical Kerr effect; optical properties of semi-infinite bulk materials; surface magnetism

## I. INTRODUCTION

The magneto-optical Kerr effect which occurs when using a rotating magnetic field (ROTMOKE) is an adequate tool to experimentally determine magnetic anisotropies. [1]

In a previous paper [2] it has been shown that at least in the case of bcc Ni/Ni(100) the approximate expression of Kerr angles widely used by experimentalists to interpret ROTMOKE data, [3] completely agrees with our *ab initio* Kerr calculations performed by means of Luttinger's formalism using a contour integration [4] within the spin-polarized relativistic screened Korringa-Kohn-Rostoker (SKKR) method [5] and applying a  $2 \times 2$  matrix technique, [6] which includes all multiple reflections and optical interferences. Furthermore, from our *ab initio* Kerr data, we concluded that the surface contributes up to 75% of the Kerr rotation angle, and hence the experimentally deduced magnetic properties cannot unambiguously be ascribed to bcc bulk Ni.

The results in Ref. [2] were obtained by comparing the Kerr angles obtained via the  $2 \times 2$  matrix technique with those arising from the two-media approach [7]. Besides providing further details of this comparison, in the present contribution macroscopic modeling of a layered system with a surface beyond the two-media approach will be suggested by investigating again the magneto-optical properties of bcc Ni/Ni(100) by means of a three-media approach, which contrary to the two-media approach also correctly accounts for the interface between the layered system and substrate.

## II. THEORETICAL AND COMPUTATIONAL FRAMEWORK

From an optical point of view, each atomic layer  $p$  is assumed to be a homogeneous, linear and anisotropic conducting medium, see Fig. 1, characterized by a complex permittivity tensor  $\tilde{\epsilon}^p(\omega)$ , which within the Gaussian system of units is given by

$$\tilde{\epsilon}^p(\omega) = \mathbf{I} + \frac{4\pi i}{\tilde{\omega}} \tilde{\sigma}^p(\omega) , \quad (1)$$

where  $\mathbf{I}$  is the  $3 \times 3$  identity matrix and  $\tilde{\omega} = \omega - i\delta$  is a complex frequency,  $\delta$  being the life-time broadening.

The layer-resolved optical conductivities  $\tilde{\sigma}^p(\omega)$ , on the other hand, are directly obtained [8] from the inter- and intra-layer contributions  $\tilde{\sigma}^{pq}(\omega)$  to the optical conductivity tensor,

$$\tilde{\sigma}^p(\omega) = \sum_{q=1}^N \tilde{\sigma}^{pq}(\omega) , \quad (p = 1, \dots, N) . \quad (2)$$

Here and in the following, layers are numbered starting with the first ( $p = 1$ ) on top of a semi-infinite substrate, such that if  $N$  layers are considered, the index of the most upper (surface) layer is given by  $p = N$ . It is also convenient to label the substrate and the vacuum by 0 and  $N + 1$ , respectively.

These layer-resolved optical conductivities are computed by applying a contour integration technique, [4] applying the SKKR method [5]. All results presented here were obtained for a photon energy  $\omega = 0.144$  Ryd  $\simeq 1.9592$  eV, i.e., for a wave length  $\lambda = 632.824 \simeq 633$  nm typical for a He-Ne laser. For further computational details see Ref. 9.

The layer-resolved permittivities in Eq. (1) serve then as input for our  $2 \times 2$  matrix technique. [6] Within such a multiscale approach, the normal modes of the electric and magnetic transverse plane waves propagating in a layer  $p$  are calculated by solving the Fresnel (characteristic) equation. For each of these normal modes then the Helmholtz equation is solved to get the electric field, which in turn yields the magnetic field by solving the curl Maxwell equation.

In practice, however, the determination of the electric field components in a layer is complicated by the fact that the Helmholtz equation has to be solved for a given normal mode by keeping at least one Cartesian component of the electric field arbitrary. But by taking into account the continuity of the tangential components of the total electric and magnetic field at the lower boundary  $z_p$  ( $p = 1, \dots, N + 1$ ), see also Fig. 1, the layer-resolved reflectivity matrix, which relates all arbitrary electric field components to each other, can be determined recursively by starting from the vanishing reflectivity matrix of the substrate. In vacuum, where there are only two normal modes, namely an incident and a reflected one, the surface reflectivity matrix relates the reflected electric field components to that of the incident ones. Thus once the recursive procedure has been terminated a determination of Kerr angles is a simple geometric task.

### III. MACROSCOPIC MODELS

All macroscopic models, which from an optical point of view approximate reasonably well any semi-infinite layered system, try to reduce the number of interfaces to account for, when describing the occurring multiple reflections and optical interferences. Common to all these optical models, however, is the presence of a semi-infinite substrate of known permittivity  $\tilde{\epsilon}^0$ . Because there are no interfaces in the substrate of thickness  $d_0 = +\infty$ , its reflectivity matrix  $\mathcal{R}_0 = 0$ .

### A. Two-media approach

The simplest and most commonly used macroscopic model approximates a multilayered system as a homogeneous, anisotropic, semi-infinite medium such that the incident light is reflected only from the interface between the layered system and the vacuum. In a finite periodic layered system one assumes that all layers have identical layer-resolved permittivities, which have to be matched properly to a semi-infinite substrate of the same material. This implies that also the permittivity of the layered system has to be identical with the permittivity of the substrate. Therefore, within the two-media approach one formally deals with  $N = 0$  layers. In the case of a homogeneous layered system consisting of identical layers it has been shown elsewhere [7] that at least for polar geometry and normal incidence the two-media approach yields the well-known Fresnel formula for the complex reflectivity coefficients, i.e., the two-media approach is in fact a limiting case of the  $2 \times 2$  matrix technique. In all other cases, however, the two-media approach strongly underestimates the Kerr angles, e.g., in polar geometry for oblique incidence.

In contrast to the  $2 \times 2$  matrix technique, within the two-media approach one cannot account for the magneto-optical activity of the semi-infinite substrate. Therefore the difference in Kerr angles between these two approaches unambiguously reveals the contribution of the surface to the magneto-optical Kerr effect, see Fig. 2. As can be seen from this figure, the surface contributions are not only extremely significant, but do represent the major part of the magnitude of the Kerr angles.

The Fresnel coefficients are introduced by

$$\begin{cases} \theta_K = \theta_K^l m_l + \theta_K^q m_l m_t \\ \varepsilon_K = \varepsilon_K^l m_l + \varepsilon_K^q m_l m_t \end{cases}, \quad (3)$$

where the normalized longitudinal and transverse components of the in-plane uniform magnetization  $\vec{M}$  are written as

$$\begin{cases} m_l = \sin \varphi_{\vec{M}} \\ m_t = \cos \varphi_{\vec{M}} \end{cases}, \quad (4)$$

in terms of the polar angle  $\varphi_{\vec{M}}$  between  $\vec{M}$  and the x axis. A comparison of the Fresnel coefficients obtained by using the two-media approach with respect to those obtained by means of the  $2 \times 2$  matrix technique, show a relatively good agreement only for the quadratic coef-

1  
2  
3  
4  
5  
6  
7  
8  
9  
10  
11  
12  
13  
14  
15  
16  
17  
18  
19  
20  
21  
22  
23  
24  
25  
26  
27  
28  
29  
30  
31  
32  
33  
34  
35  
36  
37  
38  
39  
40  
41  
42  
43  
44  
45  
46  
47  
48  
49  
50  
51  
52  
53  
54  
55  
56  
57  
58  
59  
60

ficients. This in turn implies that the quadratic Fresnel coefficients are influenced very little by the surface. On the other hand, a detailed analysis of the linear Fresnel coefficients showed that approximately 75 % arise exclusively from the surface (Fig. 3).

### B. Three-media approach

Replacing the layered system by a homogeneous, linear and anisotropic conducting medium of permittivity

$$\tilde{\epsilon}(\omega) = \frac{1}{N} \sum_{p=1}^N \tilde{\epsilon}^p(\omega) , \quad (5)$$

with  $\tilde{\epsilon}^p(\omega)$  being defined as in Eq. (1), the surface is properly accounted for, although  $N - 1$  interfaces are eliminated. It has been shown elsewhere [7] that only Eq. (5) yields a physically meaningful total permittivity in accordance with the concept of layer-resolved permittivities.

The resulting three-media approach then comprises (1) the vacuum, (2) an optically homogenized medium at least as large as the layered system,

$$d_t = \sum_{p=1}^N d_p , \quad (6)$$

and (3) the substrate in order to model the multiple reflections and optical interferences. Therefore, in contrast to the two-media approach, which fails when applied to strongly inhomogeneous layered systems [10], the three-media approach can be expected to work properly for such systems. Even though we take into consideration Eq. (6), the Kerr angles obtained by the three-media approach still fail to reproduce the Kerr angles calculated by applying the  $2 \times 2$  matrix technique. Indeed, as one can see from Fig. 4, there are, although rather small, differences with respect to  $2 \times 2$  matrix technique. From this comparison it seems that the multiple interfaces within the bcc Ni/Ni(100) layered system contribute about 25 % to the Kerr angles.

Independent of the angle of incidence  $\theta$  there are only minor differences in the Kerr angles, when calculated within the two- and three-media approach provided that the homogeneous block used as a model for the layered system is only one layer thick in both approaches,

$$d_{\perp} = \frac{1}{N} \sum_{p=1}^N d_p \equiv \frac{d_t}{N} . \quad (7)$$

Therefore it can be concluded that at least in the case of bcc Ni/Ni(100), the three-media approach incorporates the two-media approach, if the thickness of the homogenized layered system equals the perpendicular lattice spacing  $d_{\perp}$ . On the other hand, if one compares the

1  
2  
3 Kerr angles obtained within the three-media approach for two different thicknesses of the  
4 layered system, such as  $d_1 \equiv d_t = N \times d_\perp$  (with  $N$  being the total number of layers) and  
5  $d_1 \equiv d_\perp = a/2$ , see Fig. 5, small differences can be observed. This particular feature suggests  
6 that the three-media Kerr angles do depend on the thickness  $d_1$  of the homogenized layered  
7 system. Thus, it is to expect that whenever  $d_1 \neq d_\perp$ , the three-media Kerr data will always  
8 differ from those obtained via the two-media approach.  
9

10 Analyzing Fig. 6 it is obvious that the thickness-dependence of the Kerr rotation angle is  
11 much stronger than that of the Kerr ellipticity angle. Surprisingly, there exist no oscillations,  
12 e.g., ABAB...-like ones, in the values of the Kerr angles, when the thickness of the homogenized  
13 block is changed by a minimal step of  $d_\perp$ . Both Kerr angles converge with respect to  $d_1$ , however,  
14 not necessarily to their value corresponding to the same incidence, when using the  $2 \times 2$  matrix  
15 technique. Because the three-media approach correctly accounts for the surface, it means that  
16 the occurring differences have to be ascribed to the presence of interfaces in-between the atomic  
17 layers. Strictly speaking, the thickness of the homogenized layered system has to be taken in  
18 the limit of  $d_1 = \infty$ , but in practice  $d_1$  is assumed to be just a couple of hundreds of  $d_\perp$  in  
19 order to obtain converged Kerr angles. For example, independent of the orientation  
20 of the in-plane uniform magnetization, one already obtains both Kerr angles exact up to  $10^{-4}$   
21 deg for  $d_1 \simeq 500 \times d_\perp$ . Therefore, the three-media approach can be considered as a realistic  
22 and practicable, however, approximate attempt to understand magneto-optical Kerr rotation  
23 in general.  
24  
25  
26  
27  
28  
29  
30  
31  
32  
33  
34  
35  
36  
37  
38

39 In the case of the Fresnel coefficients, one can see from Fig. 7 that with the exception of the  
40 linear Fresnel coefficient  $\epsilon_K^\perp$ , all other coefficients obtained by using the three-media approach  
41 are in relatively good agreement with those calculated applying the  $2 \times 2$  matrix technique.  
42  
43  
44  
45

#### 46 IV. SUMMARY

47  
48  
49 A comparison of the calculated Kerr angles via the  $2 \times 2$  matrix technique with those  
50 determined by using the two-media approach proved that the latter approach only applies for  
51 a normal incidence. For arbitrary oblique incidences, however, about 75 % of the magnitude of  
52 Kerr rotation angle arises from surface contributions. Furthermore, it was shown in terms of  
53 the three-media approach that about 25 % of the Kerr rotation angles evaluated by means of  
54 the  $2 \times 2$  matrix technique arise from the interfaces in-between the atomic layers.  
55  
56  
57  
58  
59  
60

1  
2  
3  
4  
5  
6  
7  
8  
9  
10  
11  
12  
13  
14  
15  
16  
17  
18  
19  
20  
21  
22  
23  
24  
25  
26  
27  
28  
29  
30  
31  
32  
33  
34  
35  
36  
37  
38  
39  
40  
41  
42  
43  
44  
45  
46  
47  
48  
49  
50  
51  
52  
53  
54  
55  
56  
57  
58  
59  
60

**Acknowledgments**

One of us, C.E., wishes to acknowledge financial support from the Austrian Science Foundation (FWF, Project Number WK W004).

For Peer Review Only

- 
- 1  
2  
3  
4  
5  
6  
7 [1] R. Mattheis and G. Quednau, *phys. stat. sol. (a)* **172**, R7 (1999); *J. Magn. Magn. Mater.* **205**,  
8 143 (1999).  
9  
10 [2] C. Etz, A. Vernes, L. Szunyogh and P. Weinberger, *Phys. Rev. B* **77**, 064420 (2008).  
11  
12 [3] C. S. Tian, D. Qian, D. Wu, R. H. He, Y. Z. Wu, W. X. Tang, L. F. Yin, Y. S. Shi, G. S. Dong,  
13 X. F. Jin, X. M. Jiang, F. Q. Liu, H. J. Qian, K. Sun, L. M. Wang, G. Rossi, Z. Q. Qiu, and J.  
14 Shi, *Phys. Rev. Letters* **94**, 137210 (2005).  
15  
16 [4] L. Szunyogh and P. Weinberger, *J. Phys.: Condensed Matter* **11**, 10451 (1999); A. Vernes, L.  
17 Szunyogh, and P. Weinberger, *Phase Transitions* **75**, 167 (2002).  
18  
19 [5] J. Zablouil, R. Hammerling, L. Szunyogh, and P. Weinberger, *Electron Scattering in Solid Mat-*  
20 *ter: A Theoretical and Computational Treatise, Solid-State Sciences* (Springer Verlag, Berlin,  
21 2005).  
22  
23 [6] A. Vernes and P. Weinberger, *Phys. Rev. B* **70**, 13 4411 (2004).  
24  
25 [7] A. Vernes, L. Szunyogh, and P. Weinberger, *Phys. Rev. B* **66**, 21 4404 (2002).  
26  
27 [8] A. Vernes, L. Szunyogh, L. Udvardi, and P. Weinberger, *J. Magn. Magn. Mater.* **240**, 215 (2002).  
28  
29 [9] A. Vernes, *Philos. Mag.* **86**, 1973 (2006).  
30  
31 [10] A. Vernes, L. Szunyogh, and P. Weinberger, *Phys. Rev. B* **65**, 14 4448 (2002).  
32  
33  
34  
35  
36  
37  
38  
39  
40  
41  
42  
43  
44  
45  
46  
47  
48  
49  
50  
51  
52  
53  
54  
55  
56  
57  
58  
59  
60

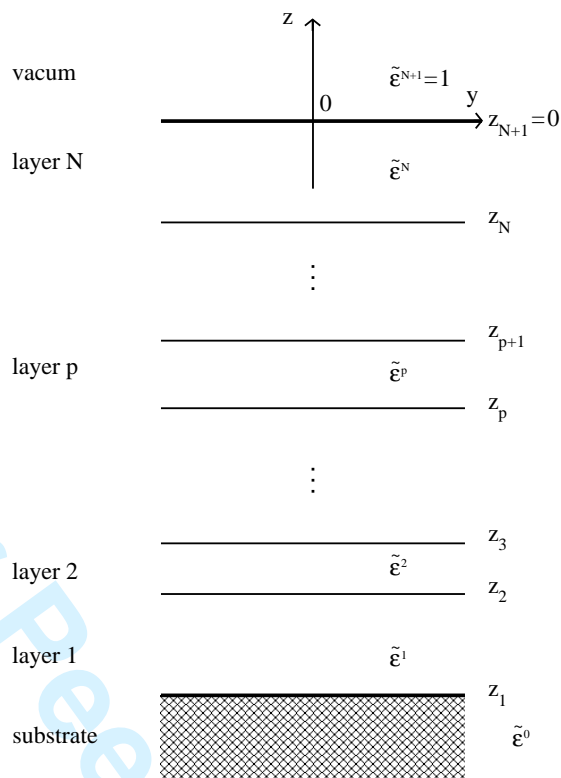


FIG. 1: The macroscopic model of a layered system used within the  $2 \times 2$  matrix technique. Not shown here is the  $0x$  axis perpendicular to the plane of the figure.

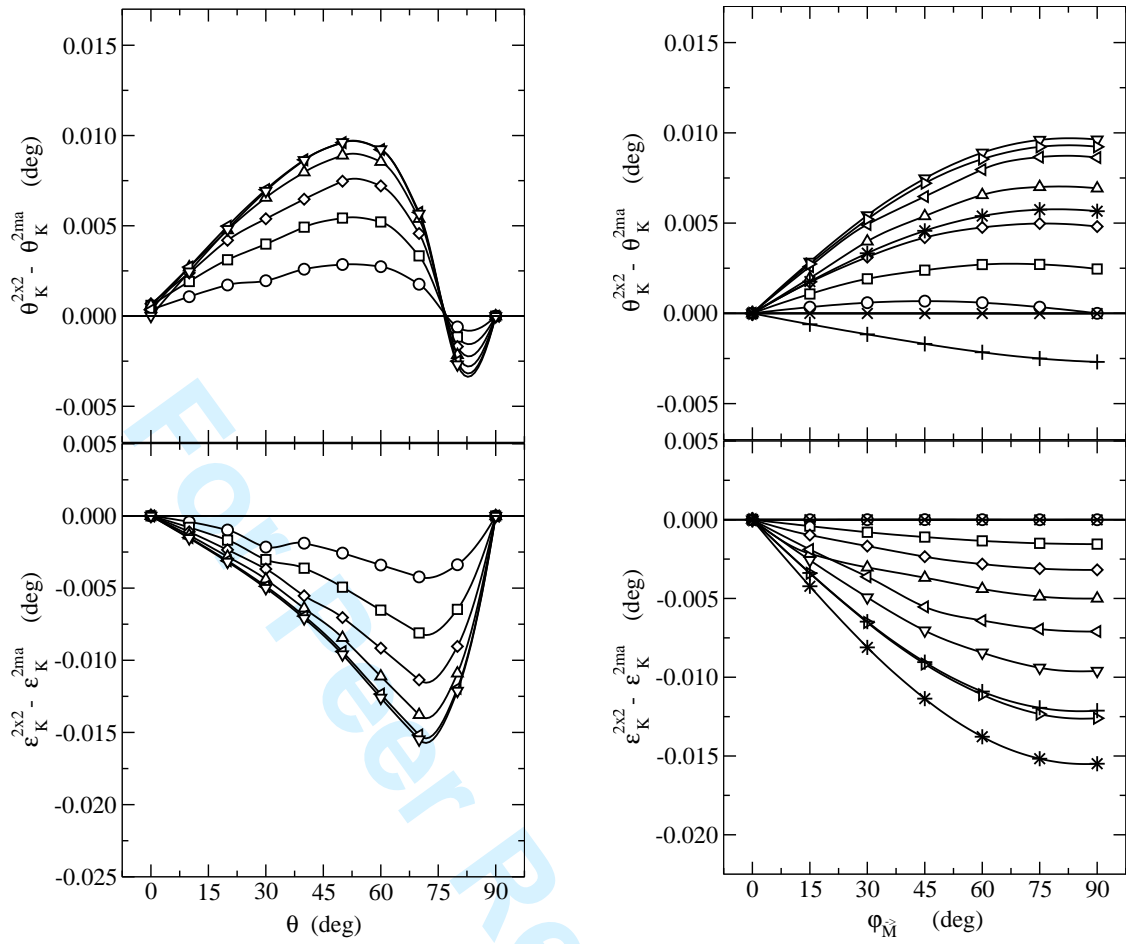


FIG. 2: Differences in the Kerr angles for oblique incidence of a  $p$ -polarized light in  $0yz$  plane ( $\lambda \simeq 633$  nm) and bcc Ni/Ni(100), when using the  $2 \times 2$  matrix technique and the two-media approach, as a function of the incidence angle  $\theta$  (left) or the polar angle  $\varphi_{\vec{M}}$  providing the direction of the in-plane uniform magnetization with respect to the  $0x$  axis (right). In the left panel circles, squares, diamonds and triangles (up, left and down) refer to Kerr angles obtained for a polar angle  $\varphi_{\vec{M}} = 15^\circ, 30^\circ, 45^\circ, 60^\circ, 75^\circ, 90^\circ$  (open symbols), in the right panel circles, squares, diamonds and triangles (up, left, down and right) represent Kerr angles obtained for an angle of incidence  $\theta = 0, 10, \dots, 60^\circ$  (open symbols), stars, pluses and crosses stand for  $\theta = 70^\circ, 80^\circ, 90^\circ$ .

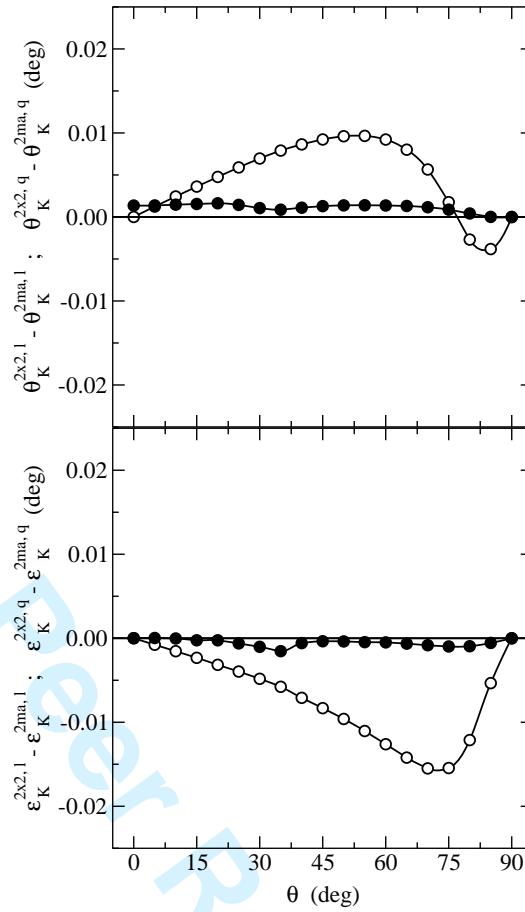


FIG. 3: Difference in the Fresnel coefficients for a  $p$ -polarized light within the  $0yz$  plane ( $\lambda \simeq 633$  nm) for bcc Ni/Ni(100), when using the  $2 \times 2$  matrix technique and the two-media approach, as a function of the incidence angle  $\theta$ . Difference in linear and quadratic Fresnel coefficients are represented by open and full circles.

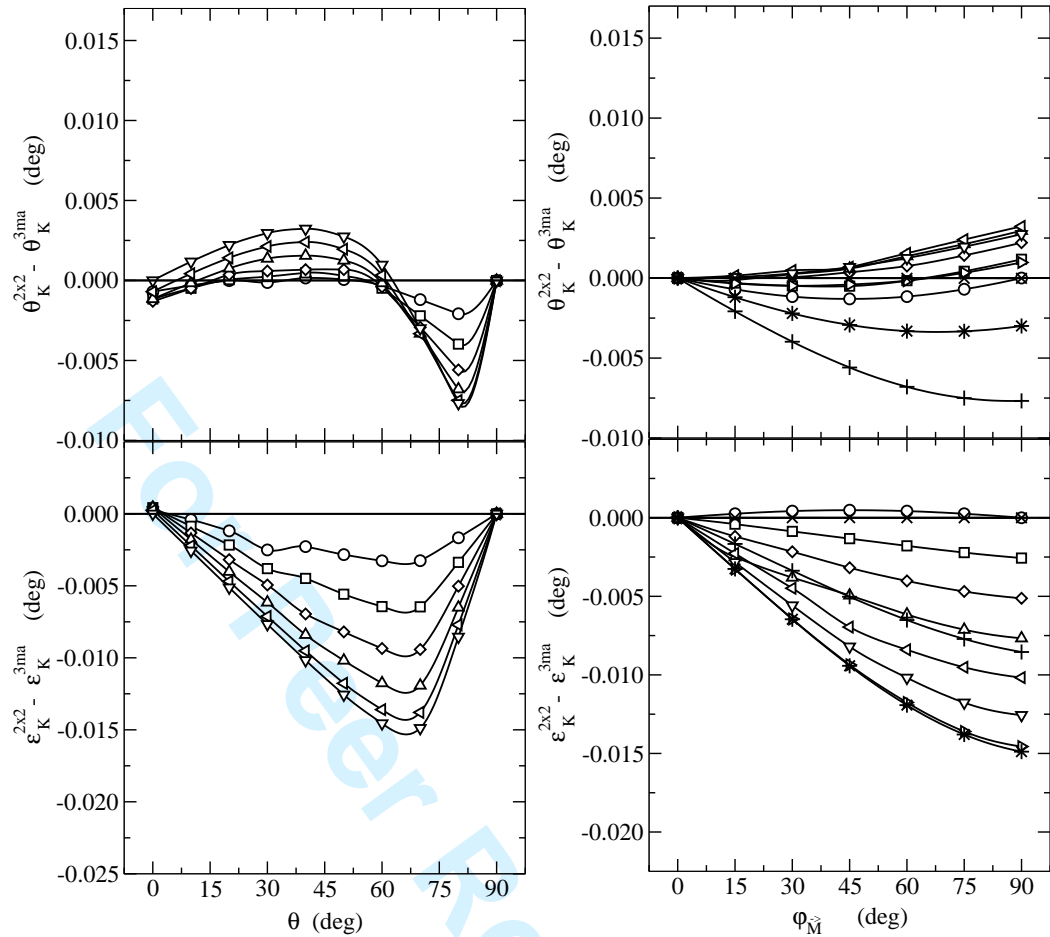


FIG. 4: Differences in the Kerr angles for oblique incidence in the case of a  $p$ -polarized light in  $Oyz$  plane ( $\lambda \simeq 633$  nm) for bcc Ni/Ni(100) when using either the  $2 \times 2$  matrix technique or the three-media approach as a function of the incidence angle  $\theta$  or the polar angle  $\varphi_{\vec{M}}$ . In the left panel: circles, squares, diamonds and triangles (up, left and down) mark Kerr angles obtained for a polar angle  $\varphi_{\vec{M}} = 15^\circ, 30^\circ, 45^\circ, 60^\circ, 75^\circ, 90^\circ$  (open symbols). In the right panel: circles, squares, diamonds and triangles (up, left, down and right) stand for Kerr angles obtained for an angle of incidence  $\theta = 0, 10, \dots, 60^\circ$  (open symbols), whereas stars, pluses and crosses represent an incidence at  $\theta = 70^\circ, 80^\circ, 90^\circ$ .

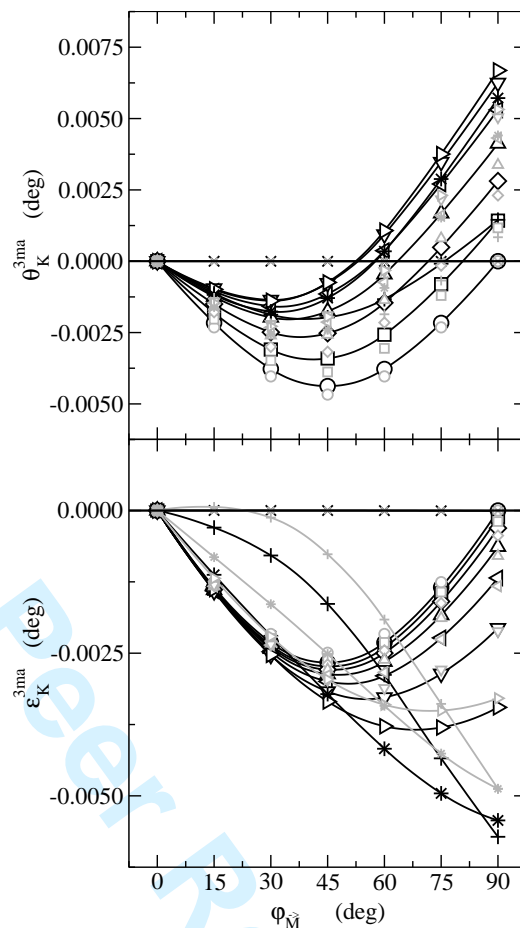


FIG. 5: Kerr angles for oblique incidence in the case of a  $p$ -polarized light in  $0yz$  plane ( $\lambda \simeq 633$  nm) for bcc Ni/Ni(100) when using the three-media approach with an effective thickness of the homogenized layered system  $d_1 \equiv d_t = N \times d_\perp$  (black) and  $d_1 \equiv d_\perp = a/2$  (grey), i.e., equal to the perpendicular lattice spacing for a lattice constant  $a = 5.329$  a.u. as a function of the polar angle  $\varphi_{\vec{M}}$ . ( $N$  denotes the total number of layers.) Circles, squares, diamonds and triangles (up, left, down and right) mark Kerr angles obtained for an angle of incidence  $\theta = 0, 10, \dots, 60^\circ$  (open symbols), whereas stars, pluses and crosses stand for  $\theta = 70^\circ, 80^\circ, 90^\circ$ .

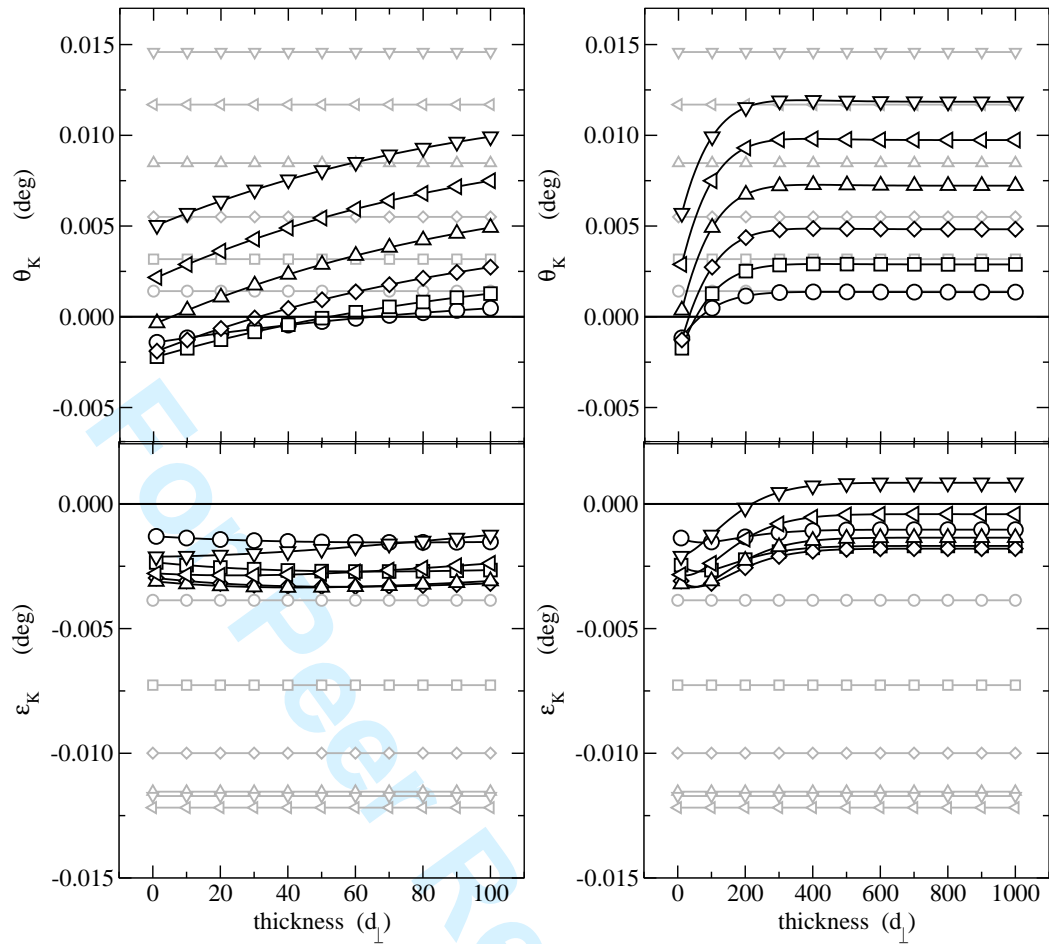


FIG. 6: Kerr angles for an incidence angle  $\theta = 50^\circ$  in the case of a  $p$ -polarized light in  $Oyz$  plane ( $\lambda \simeq 633$  nm) for bcc Ni/Ni(100) when using the three-media approach as a function of the thickness  $d_\perp$  of the homogenized layered system in units of the perpendicular lattice spacing  $d_\perp = a/2$  (black) for  $a = 5.329$  a.u. . Circles, squares, diamonds and triangles (up, left and down) represent Kerr angles obtained for a polar angle  $\varphi_{\vec{M}} = 15^\circ, 30^\circ, 45^\circ, 60^\circ, 75^\circ, 90^\circ$ . Horizontal grey lines mark the corresponding Kerr angles obtained by applying the  $2 \times 2$  matrix technique.

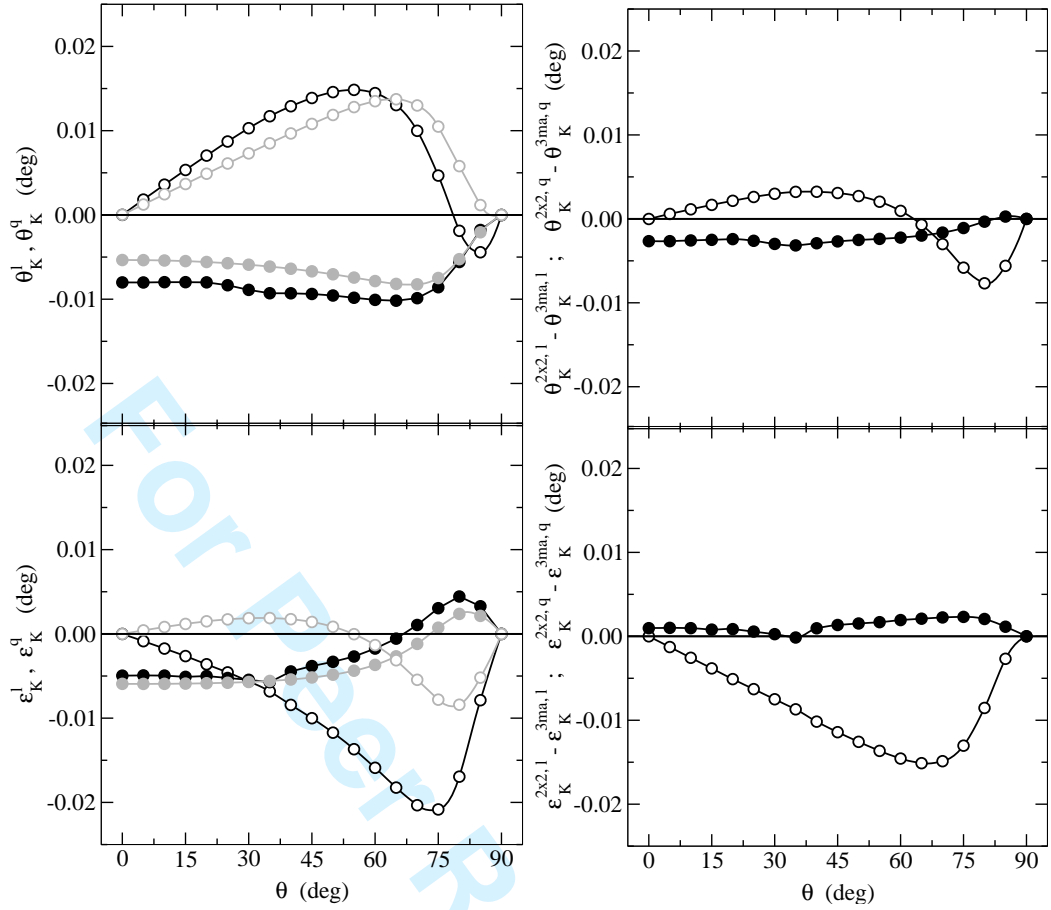
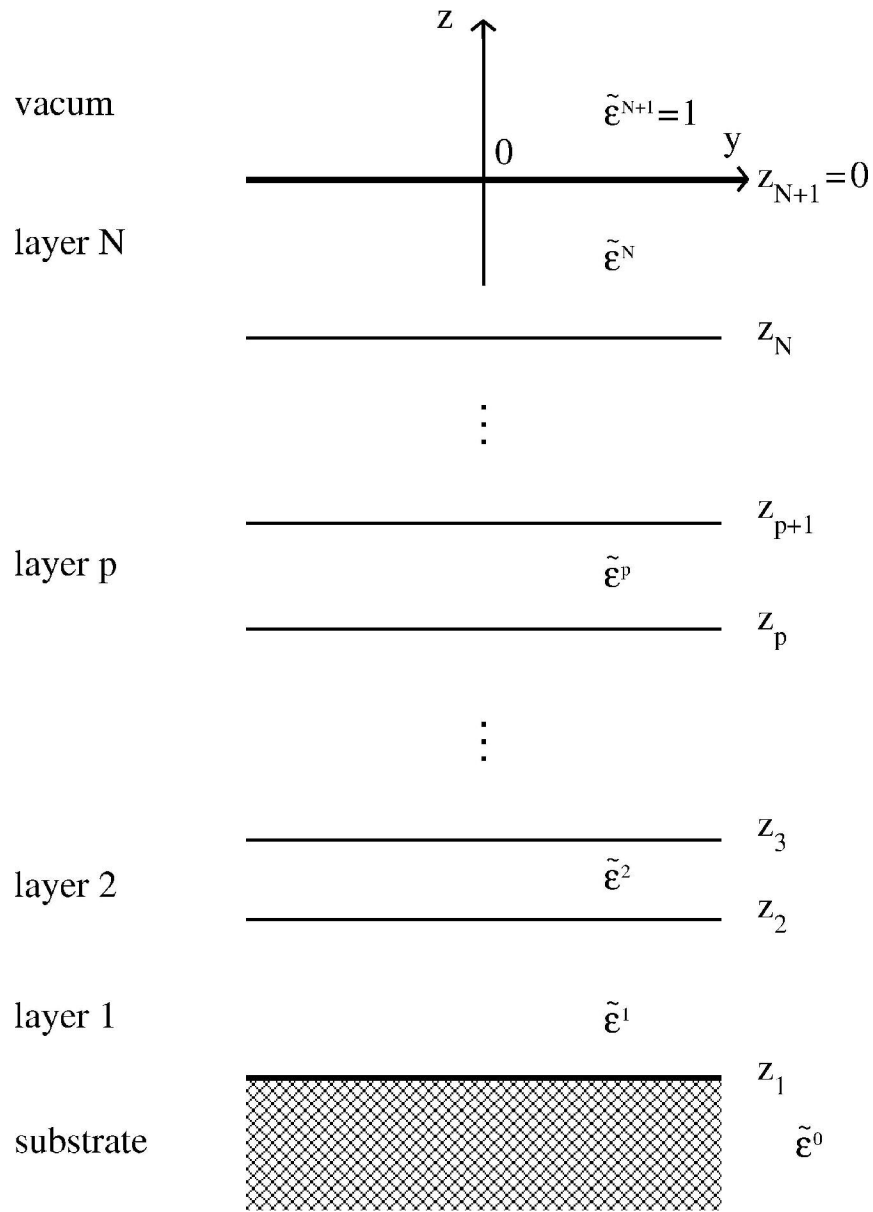


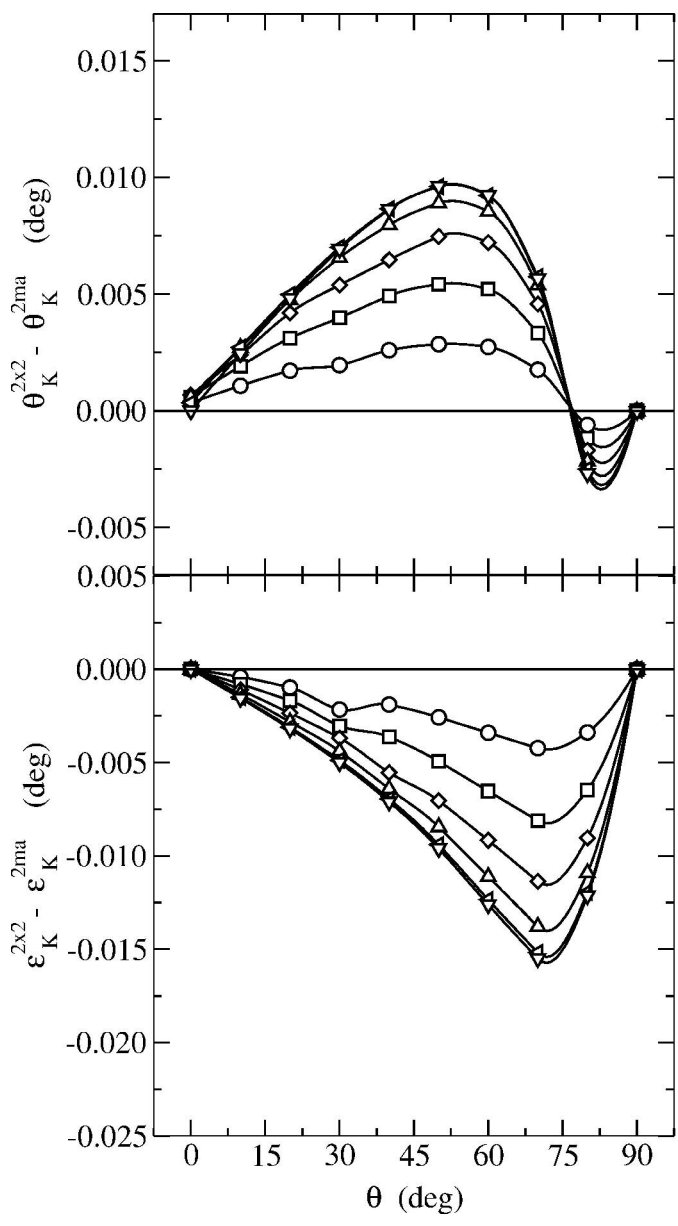
FIG. 7: Fresnel coefficients for a  $p$ -polarized light within the  $0xy$  plane ( $\lambda \simeq 633$  nm) for bcc Ni/Ni(100) when using the  $2 \times 2$  matrix technique (black) and the three-media approach with  $d_1 = \infty$  (grey), respectively, as a function of the incidence angle  $\theta$ , left panel. Linear and quadratic Fresnel coefficients are represented by open and full circles. In the right panel, the differences in the Fresnel coefficients are depicted.

1  
2  
3  
4  
5  
6  
7  
8  
9  
10  
11  
12  
13  
14  
15  
16  
17  
18  
19  
20  
21  
22  
23  
24  
25  
26  
27  
28  
29  
30  
31  
32  
33  
34  
35  
36  
37  
38  
39  
40  
41  
42  
43  
44  
45  
46  
47  
48  
49  
50  
51  
52  
53  
54  
55  
56  
57  
58  
59  
60

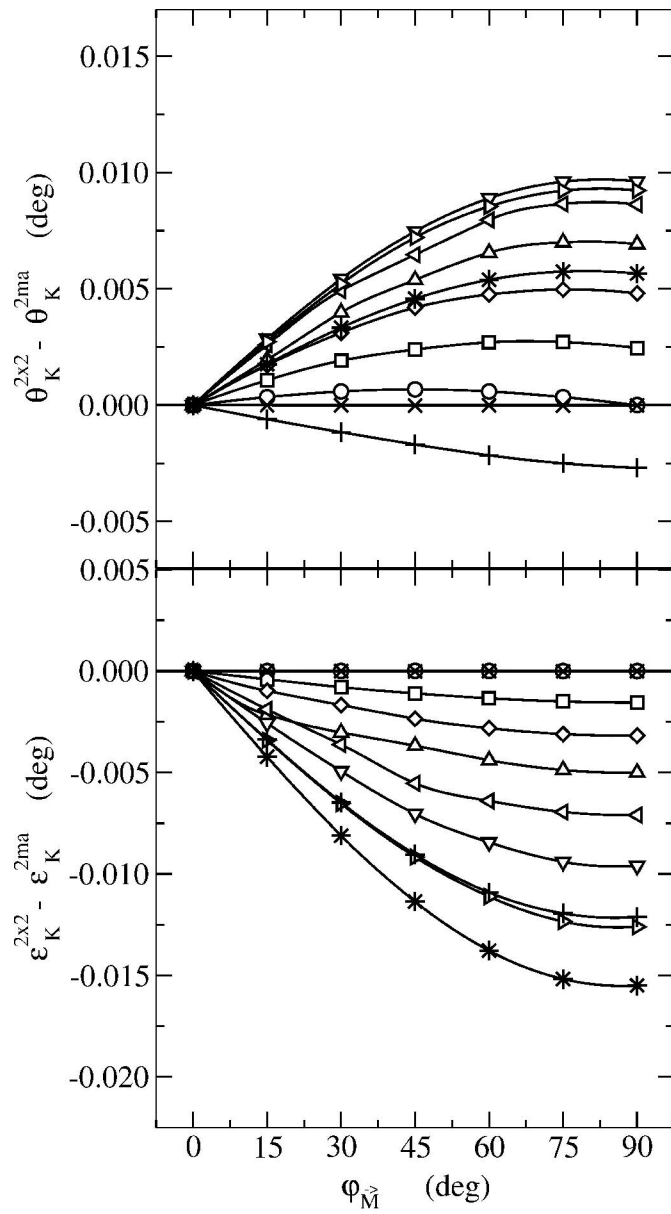


102x144mm (600 x 600 DPI)

1  
2  
3  
4  
5  
6  
7  
8  
9  
10  
11  
12  
13  
14  
15  
16  
17  
18  
19  
20  
21  
22  
23  
24  
25  
26  
27  
28  
29  
30  
31  
32  
33  
34  
35  
36  
37  
38  
39  
40  
41  
42  
43  
44  
45  
46  
47  
48  
49  
50  
51  
52  
53  
54  
55  
56  
57  
58  
59  
60

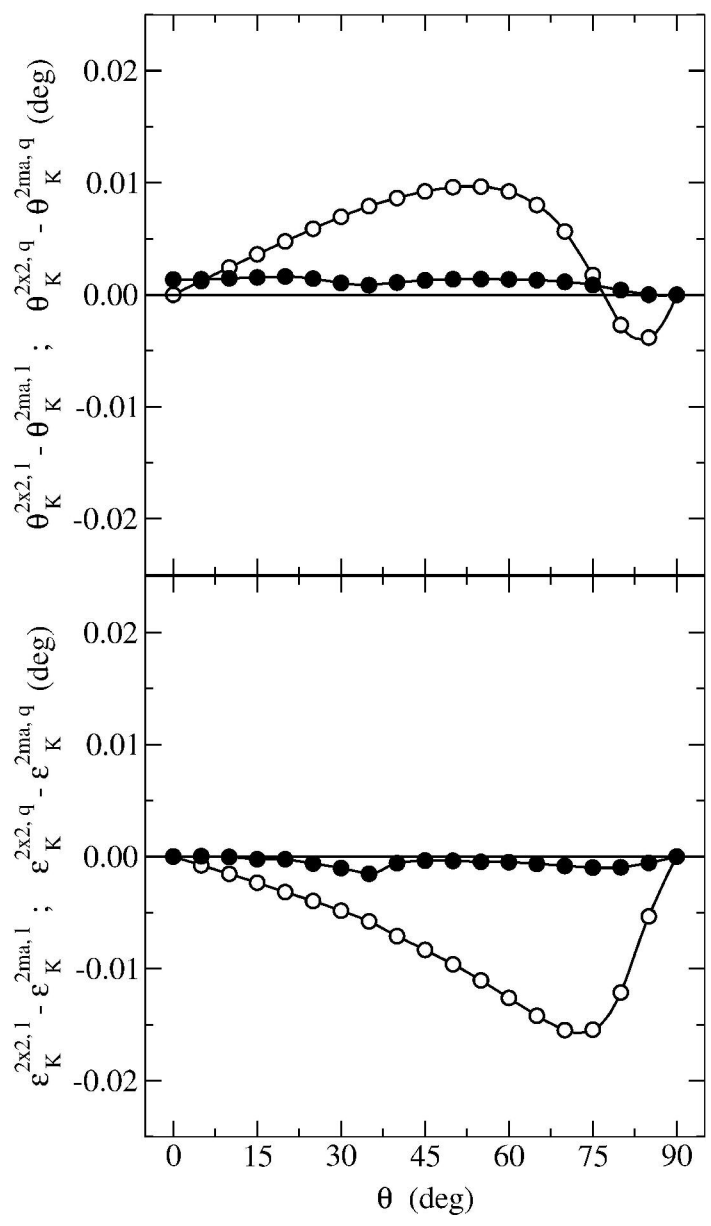


135x244mm (600 x 600 DPI)

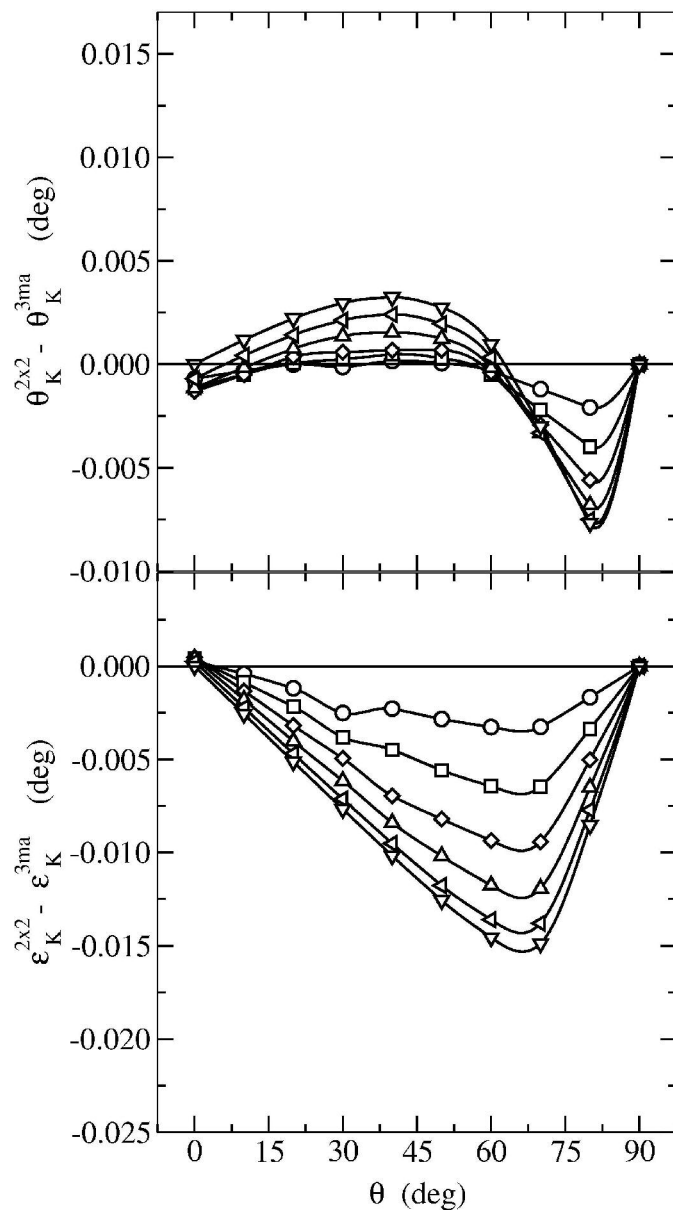


135x244mm (600 x 600 DPI)

1  
2  
3  
4  
5  
6  
7  
8  
9  
10  
11  
12  
13  
14  
15  
16  
17  
18  
19  
20  
21  
22  
23  
24  
25  
26  
27  
28  
29  
30  
31  
32  
33  
34  
35  
36  
37  
38  
39  
40  
41  
42  
43  
44  
45  
46  
47  
48  
49  
50  
51  
52  
53  
54  
55  
56  
57  
58  
59  
60



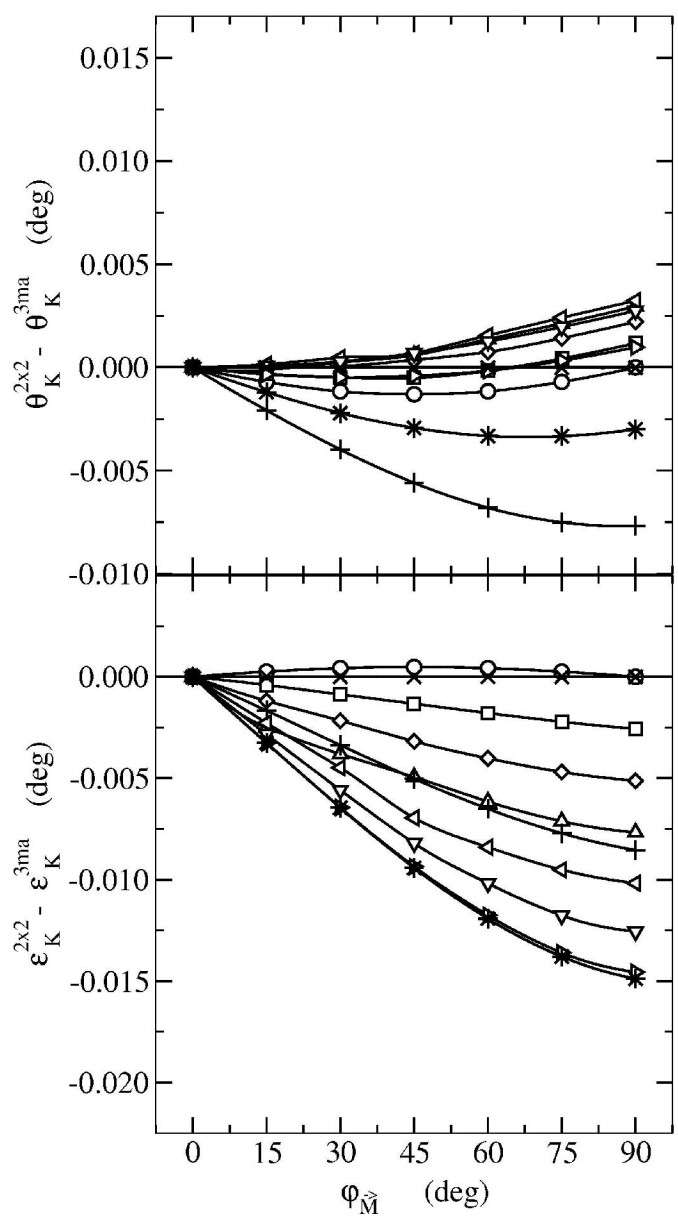
135x234mm (600 x 600 DPI)



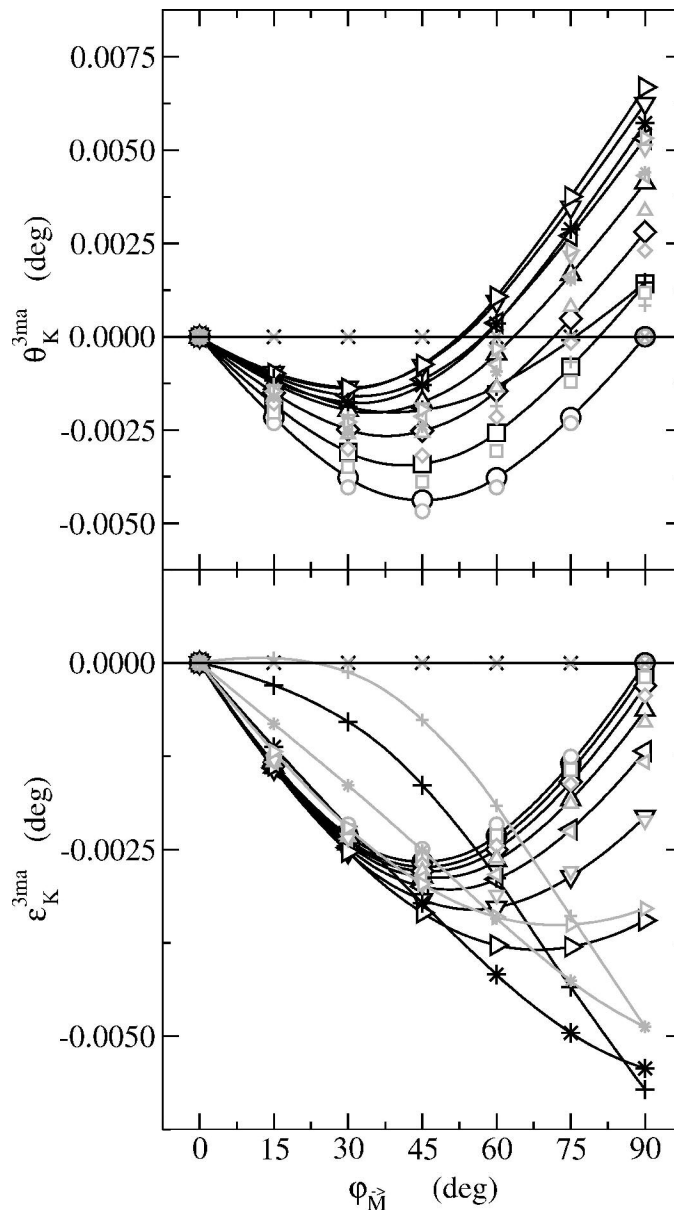
76x137mm (600 x 600 DPI)

1  
2  
3  
4  
5  
6  
7  
8  
9  
10  
11  
12  
13  
14  
15  
16  
17  
18  
19  
20  
21  
22  
23  
24  
25  
26  
27  
28  
29  
30  
31  
32  
33  
34  
35  
36  
37  
38  
39  
40  
41  
42  
43  
44  
45  
46  
47  
48  
49  
50  
51  
52  
53  
54  
55  
56  
57  
58  
59  
60

1  
2  
3  
4  
5  
6  
7  
8  
9  
10  
11  
12  
13  
14  
15  
16  
17  
18  
19  
20  
21  
22  
23  
24  
25  
26  
27  
28  
29  
30  
31  
32  
33  
34  
35  
36  
37  
38  
39  
40  
41  
42  
43  
44  
45  
46  
47  
48  
49  
50  
51  
52  
53  
54  
55  
56  
57  
58  
59  
60

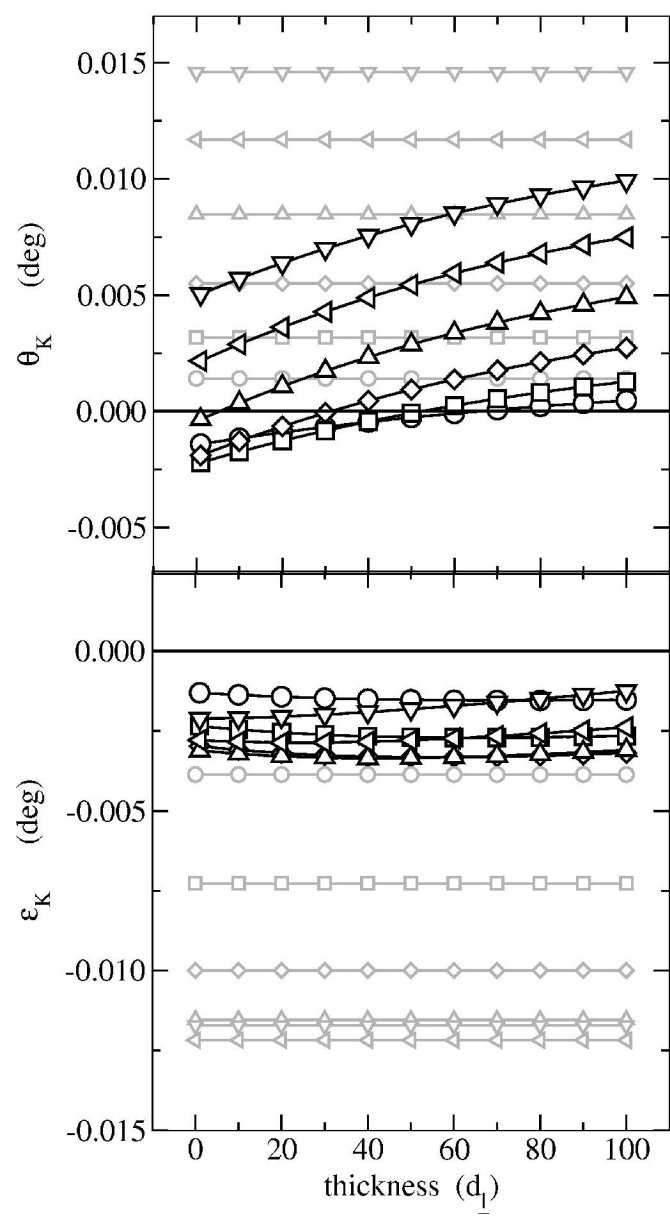


76x137mm (600 x 600 DPI)

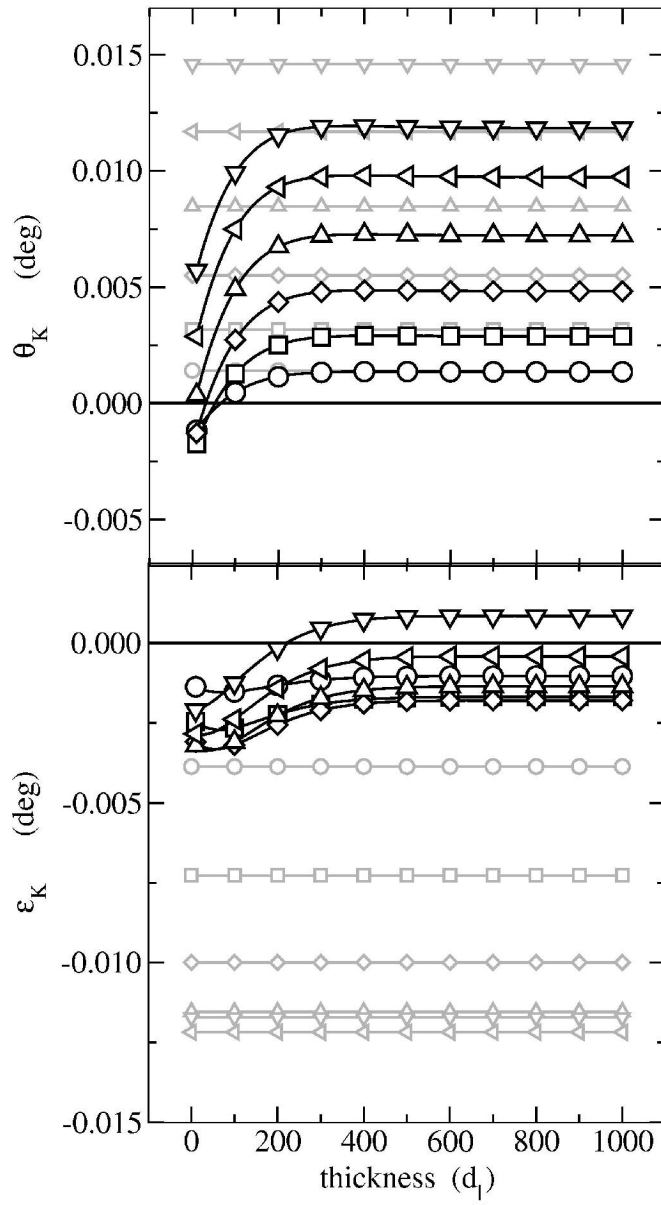


135x241mm (600 x 600 DPI)

1  
2  
3  
4  
5  
6  
7  
8  
9  
10  
11  
12  
13  
14  
15  
16  
17  
18  
19  
20  
21  
22  
23  
24  
25  
26  
27  
28  
29  
30  
31  
32  
33  
34  
35  
36  
37  
38  
39  
40  
41  
42  
43  
44  
45  
46  
47  
48  
49  
50  
51  
52  
53  
54  
55  
56  
57  
58  
59  
60



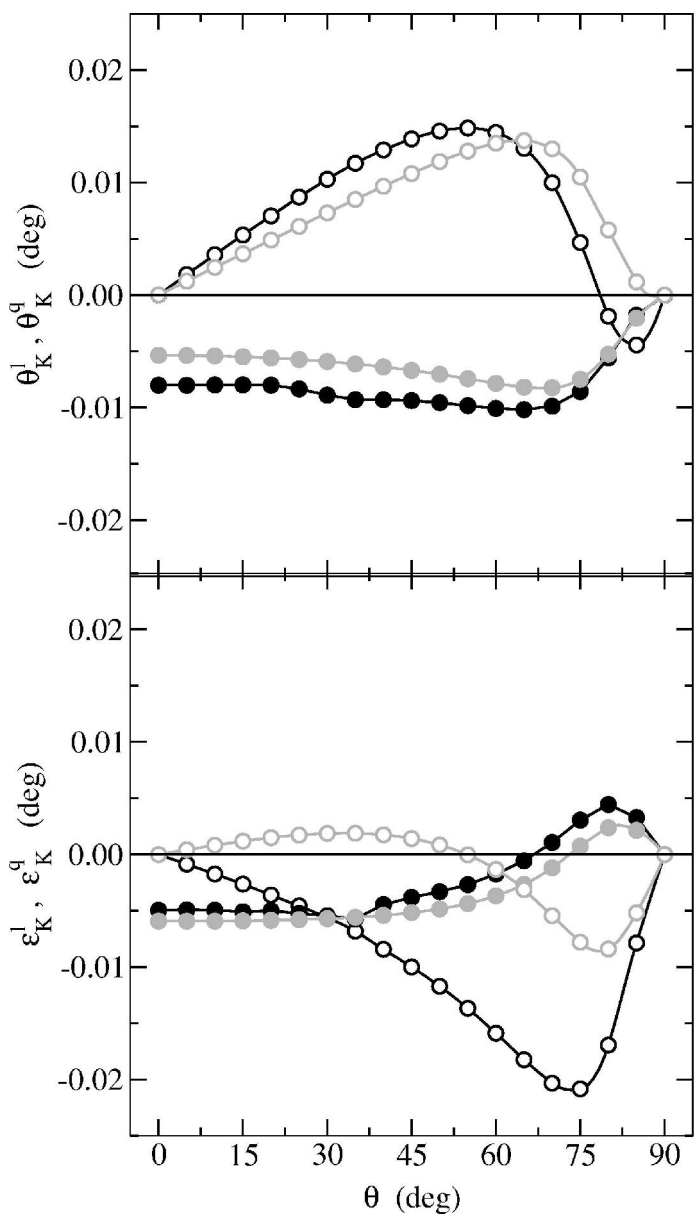
76x138mm (600 x 600 DPI)



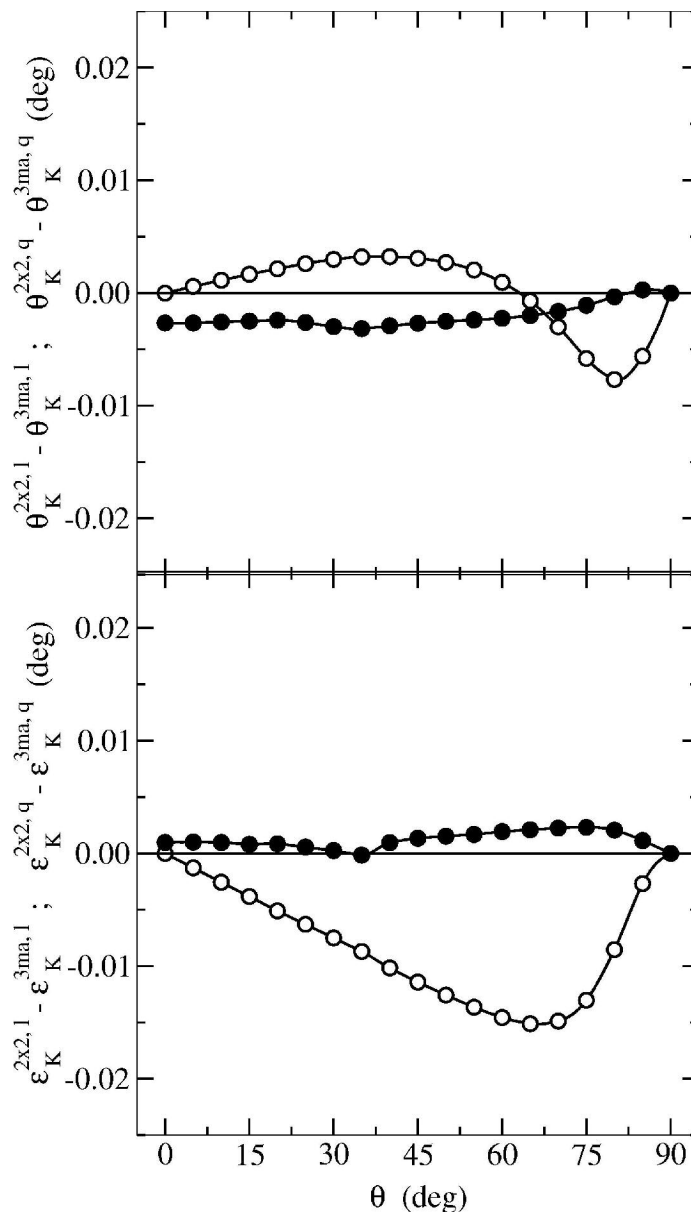
76x138mm (600 x 600 DPI)

1  
2  
3  
4  
5  
6  
7  
8  
9  
10  
11  
12  
13  
14  
15  
16  
17  
18  
19  
20  
21  
22  
23  
24  
25  
26  
27  
28  
29  
30  
31  
32  
33  
34  
35  
36  
37  
38  
39  
40  
41  
42  
43  
44  
45  
46  
47  
48  
49  
50  
51  
52  
53  
54  
55  
56  
57  
58  
59  
60

1  
2  
3  
4  
5  
6  
7  
8  
9  
10  
11  
12  
13  
14  
15  
16  
17  
18  
19  
20  
21  
22  
23  
24  
25  
26  
27  
28  
29  
30  
31  
32  
33  
34  
35  
36  
37  
38  
39  
40  
41  
42  
43  
44  
45  
46  
47  
48  
49  
50  
51  
52  
53  
54  
55  
56  
57  
58  
59  
60



76x133mm (600 x 600 DPI)



76x132mm (600 x 600 DPI)

1  
2  
3  
4  
5  
6  
7  
8  
9  
10  
11  
12  
13  
14  
15  
16  
17  
18  
19  
20  
21  
22  
23  
24  
25  
26  
27  
28  
29  
30  
31  
32  
33  
34  
35  
36  
37  
38  
39  
40  
41  
42  
43  
44  
45  
46  
47  
48  
49  
50  
51  
52  
53  
54  
55  
56  
57  
58  
59  
60